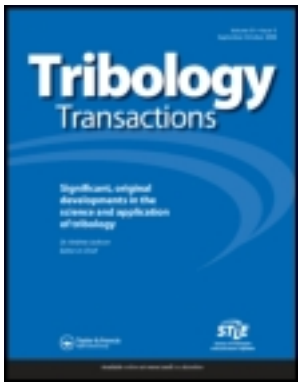


Tribology Transactions
Publication details, including instructions for authors and subscription information:
http://www.tandfonline.com/loi/utrb20

# Wear Behavior of Carbidic Ductile Iron with Different Matrices and Carbide Distribution

Alejandro Basso [a] , Sebastian Laino [a] & Ricardo C. Dommarco [a]
[a] School of Engineering, Universidad Nacional de Mar del Plata, INTEMA-CONICET, Av. Juan B. Justo 4302, B7608FDQ, Mar del Plata, Argentina
Version of record first published: 16 Jan 2013.

To cite this article: Alejandro Basso , Sebastian Laino & Ricardo C. Dommarco (2013): Wear Behavior of Carbidic Ductile Iron with Different Matrices and Carbide Distribution, Tribology Transactions, 56:1, 33-40

To link to this article: http://dx.doi.org/10.1080/10402004.2012.725149

*Tribology Transactions, 56:* 33-40, 2013

ISSN: 1040-2004 print / 1547-397X online
DOI: 10.1080/10402004.2012.725149

STLE
Society of Tribologists and Lubrication Engineers

# Wear Behavior of Carbidic Ductile Iron with Different Matrices and Carbide Distribution

ALEJANDRO BASSO, SEBASTIAN LAINO, and RICARDO C. DOMMARCO
School of Engineering, Universidad Nacional de Mar del Plata
INTEMA–CONICET, Av. Juan B. Justo 4302
B7608FDQ, Mar del Plata, Argentina



*Similar to other mechanical properties, wear resistance is entirely dependent on a material's microstructure, which, in turn, is related to the chemical composition and solidification rate, which controls the type of phase, size, amount, and dispersion. Depending on the tribosystem, the abrasive wear resistance of ductile iron (DI) may be improved by heat treatment as well as by reinforcing the matrix with hard particles such as carbides, typically obtained by alloying with elements such as chromium.*

*The solidification rate mainly depends on wall thickness and mold characteristics. In DI, the solidification rate affects microstructural characteristics, such as nodule size, nodule count, carbide size and distribution, and matrix refinement, also including the last to freeze (LTF) amount, size, and distribution.*

*This study evaluates the influence of the wall thickness (12.5, 25, 50, and 75 mm) on the abrasion resistance and impact toughness of DI with different matrices reinforced with carbides. Carbidic structures were obtained by alloying the melt with Cr, and the different types of matrices such as pearlitic, martensitic, and ausferritic (CADI) were obtained under as-cast conditions or by heat treatment.*

*The results reflect the influence of cooling rate on the microstructural characteristics and its relationship with the mechanical properties, particularly the abrasive wear resistance. It was demonstrated that, under the present experimental conditions, the highest carbide content and matrix hardness, obtained from the 12.5-mm-thick part with a martensitic matrix, resulted in the highest abrasion resistance.*

**KEY WORDS**

Carbides; Iron; Metallurgical Analysis; XRD; Abrasive Wear

## INTRODUCTION

Cast irons have assumed greater importance among the metallic materials commonly used in the industry, due to the wide range of mechanical properties that the different casting types exhibit. White cast irons are used in applications requiring high abrasion resistance and characterized by a microstructure containing high amounts of carbides with hardness between 800 and 3000 HV, depending on the type of carbide. However, white cast irons are not only difficult to machine but also feature very low impact toughness.

Ductile irons (DIs) have a wide range of industrial applications due to their good combination of mechanical properties. In particular, austempered ductile iron (ADI) has been on the constant increase worldwidedue to its excellent combination of high tensile strength and high impact toughness (over 1,600 MPa and 100 J for grades 5 and 1, respectively, in accordance with the ASTM A897M standard), which is explained by the ausferritic matrix obtained by austempering. These properties have allowed ADI to replace forged steels in many applications. In addition, ADI has good response to different wear mechanisms, such as adhesive wear due to graphite presence, resulting in good performance when used for rolling–sliding contact conditions (Magalhaes and Seabra *(1)*; Straffelini, et al. *(2)*; Dommarco, et al. *(3)*) or abrasive wear due to its tough ausferritic matrix (Yang and Putatunda *(4)*; Dommarco, et al. *(5)*; Shepperson and Allen *(6)*).

In recent years, some researchers have focused on a new DI variant called carbidic ADI (CADI) consisting of carbides immersed in an ausferritic matrix in the presence of graphite nodules. Carbides are obtained during solidification by alloying the melt with carbide-forming elements, usually chromium. After casting, the material is heat treated by austempering in order to obtain CADI (Laino, et al. *(7)*, *(8)*). This type of DI intends to fill the gap between ADIs and white cast irons by means of a new material variant of higher abrasion resistance than ADI and higher impact toughness than white cast irons.

The abrasive wear resistance of CADI is determined by the type of phase, morphology, amount, and distribution (nodules, free carbides, and matrix microconstituents), which, in turn, for a given chemical composition, are dependent on the solidification rate and heat treatment parameters. It has been observed that, as the solidification rate decreases, fewer and larger nodules are obtained and the size of nonmetallic inclusions located in the last to freeze (LTF) zones increases. As postulated in previous works (Rebasa, et al. *(9)*; Dommarco, et al. *(10)*) for high nodule count ductile irons (above 300 nodules/mm$^2$), abrasive wear resistance decreases in laboratory tests (ASTM G65) as the nodule count

**Manuscript received May 24, 2012**
**Manuscript accepted August 21, 2012**
**Review led by Robert Errichello**

TABLE 1—HEAT TREATMENT PARAMETERS AND SAMPLE IDENTIFICATION

| Matrix | Austenizing Temperature $T_\gamma$ (°C) | Austenizing Time $t_\gamma$ (s) | Austempering Temperature $T_a$ (°C) | Austempering Time $t_a$ (s) | Identification |
|---|---|---|---|---|---|
| Pearlitic | 910 | 3,600 | — | — | PDI |
| Martensitic | 910 | 3,600 | Tempered @ 250 | 3,600 | MDI |
| Ausferritic | 910 | 7,200 | 360 | 5,400 | CADI-360 |
| Ausferritic | 910 | 7,200 | 280 | 5,400 | CADI-280 |

increases. When considering the presence of carbides, it was noticed that their occurrence could promote either higher or lower abrasion resistance depending on the tribosystem (Laino, et al. *(11)*; Ceccarelli, et al. *(12)*; Giacchi, et al. *(13)*). With respect to the matrix, it is generally accepted that higher hardness promotes higher abrasion resistance. Nevertheless, many authors observed an oposite response under different wear conditions (Laino, et al. *(14)*; Francucci, et al. *(15)*).

In view of the strong role that microstructural characteristics play on DI mechanical and wear properties, this work centers on the study of the way in which wall thickness (solidification rate) and alloying affect nodule count and carbides distribution as well as its effect on the wear properties. In particular, DI's abrasive wear resistance and impact toughness with free carbides in the microstructure and different types of matrices—pearlitic, martensitic, and ausferritic (CADI)—were explored.



## EXPERIMENTAL PROCEDURE

### Materials and Sample Preparation

A ductile iron melt was obtained in a metal casting laboratory facility using a 100-kg capacity medium-frequency induction furnace and casting in sand molds. Steel scrap and foundry returns were used as charge materials. Nodularization was conducted using the sandwich method, employing 1.5 wt% of Fe-Si-Mg (6% Mg), and inoculation was done with 0.6 wt% Fe-Si (75% Si). The melt was alloyed with small amounts of copper and nickel to ensure austemperability and with chromium to promote carbides precipitation. The liquid iron was finally cast into 12.5-, 25-, 50-, and 75-mm-thick Y-block (ASTM A395) sand molds.

### Heat Treatments

Four different matrix microstructures were evaluated: pearlitic, martensitic, and two ausferritic (CADI variants). A fully pearlitic matrix was obtained in the as-cast condition. A martensitic matrix was obtained by a quench and temper heat treatment consisting of an austenitizing step at $T_\gamma = 910°C$ for $t_\gamma = 3{,}600$ s, followed by water cooling and then tempering at $T = 250°C$ for $t = 3{,}600$ s. The two CADI variants were obtained by a heat treatment cycle consisting of an austenitizing step at $T_\gamma = 910°C$ for $t_\gamma = 7{,}200$ s and then austempering in a salt bath at $T_a = 280$ and $360°C$ for $t_a = 5{,}400$ s. Heat treatment parameters and sample identification are listed in Table 1.

### Chemical and Microstructural Analysis

Heat chemical compositionwas determined by means of a Baird spark optical emission spectrograph (DV6, INTEMCONICET, Argentina). Preparation of the metallographic samples was carried out using standard techniques for cutting and polishing. Etching was performed with 2% nital. Microstructural characterization was conducted using optical and scanning electron microscopy. The nodularity and nodule count values were measured in agreement with ASTM standard A247. For carbide quantification, samples were etched with 10% ammonium persulfate (Química Industrial Kubo) in aqueous solution and the content was measured at several random locations of the microstructure with a low optical magnification (5×) using Image-Pro Plus software.

The carbide content was evaluated under as-cast and heat-treated conditions, in order to analyze carbide dissolution during the austenitizing stage of heat treatments. Carbides were also chemically characterized by energy-dispersive spectroscopy (EDS, EDAX, INTEM-CONICET, Argentina) to evaluate differences in chemical composition arising from the different cooling rates. The values reported are the average of five measurements performed on carbides at different sample locations.

### X-Ray Diffraction Analysis

The amount of retained austenite was evaluated using X-ray diffraction (XRD) analysis on CADI-280 and CADI-360 samples surfaces under unworn ($\gamma_{UW}$) and worn ($\gamma_W$) conditions in order to evaluate the austenite-to-martensite transformation promoted by abrasion. The unworn surfaces were prepared by polishing followed by removal of the distorted material using a chemical etchant consisting of 85 parts of distilled water, 10 parts of hydrofluoric acid, and 15 parts of hydrogen peroxide. Worn surfaces were obtained after the wear tests. XRD analysis was carried out with a PANalytical X'pert PRO diffractometer (INTEM-CONICET, Argentina), using a Cu target and graphite monochromator, operating at 40 kV and 40 mA and scanning in the range of $20° < \theta < 90°$ at a speed of 1°/min. Profiles were analyzed to obtain the peak positions and the intensity of the {220} plane for the face-centered cubic austenite. The volume fraction of retained austenite was then determined by computer software (Origin 9.0) using the integrated intensities of the {220} plane for the austenite. Each reported value is the average of three individual tests corresponding to each sample condition. Fully austenitic stainless steel was used as a reference material.

### Mechanical Tests

The samples' Brinell hardness (HBW) was measured using a 2.5-mm tungsten carbide ball and a bench tester with a 187.5 kg load (ASTM E10). Microhardness was measured by the Vickers method (HV) using a 500-g load. Impact toughness was evaluated by conducting Charpy impact tests according to ASTM standard E23,using 10 × 10 × 55 mm specimens and an Amsler pendulum with an initial energy of 300 J (5 m/s impact speed). Given the characteristics of the evaluated materials, unnotched

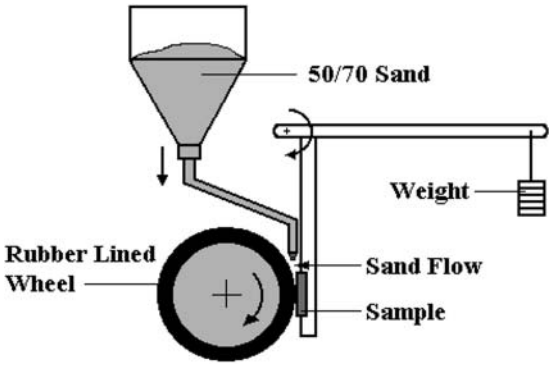


**Fig. 1—Schematic of the dry sand/rubber wheel apparatus (ASTM G65).**

samples were used. The reported values are the average of four determinations.

The abrasive wear resistance was assessed by means of the dry sand/rubber wheel abrasion test, according to ASTM standard G65 using procedure A. Figure 1 depicts a schematic of the testing machine. The relative wear resistance index, $E$, was calculated as the relation between the volume loss of a reference material, $\Delta V_R$—in this case an SAE 1010 steel—and the volume loss of the ductile iron sample, $\Delta V_S$, based on Eq. [1]:

$$E = \frac{\Delta V_R}{\Delta V_S} \quad [1]$$

Weight loss values were measured by means of a 0.1-mg precision scale and then converted into volume loss using density values of $\delta = 7.2$ and 7.8 g/cm$^3$ for iron and steel, respectively. Density values were determined using dimensionally calibrated blocks. Each $E$ value reported corresponding to the different Y-block thicknesses and metallic matrix was obtained from the average of three individual tests. The reference material was tested for each material variant studied.

## RESULTS AND DISCUSSION

### Chemical and Microstructural Characterization

The chemical composition of the heat used in this study is listed in Table 2. The equivalent carbon was CE = 4.1, giving a slightly hypoeutectic composition. The main alloying elements were Cu = 1.2%, in order to increase austemperability, and Cr = 2.0%, in order to promote carbide precipitation.

Figure 2 illustrates the as-cast microstructures of the different Y-blocks, composed of graphite nodules (black areas), free carbides (dark grey areas), and fully pearlitic matrices (light grey areas), even for the 75-mm-thick Y-blocks. In conformity with ASTM standard A247, nodularity exceeded 90% in all cases. Nodule counts were 320, 290, 140, and 80 nodules/mm$^2$, and the sizes were 7, 5, 4, and 3 for the 12.5-, 25-, 50-, and 75-mm Y-blocks, respectively.

TABLE 3—CARBIDE CONTENT IN THE AS-CAST CONDITION AND AFTER HEAT TREATMENT

| | Carbide Content (%) | |
|---|---|---|
| Y-Block Thickness (mm) | As-Cast | Heat-Treated |
| 12.5 | 26 | 22 |
| 25.0 | 22 | 19 |
| 50.0 | 19 | 17 |
| 75.0 | 14 | 14 |

Figure 3 exhibits the microstructures (optical microscopy) after etching with ammonium persulfate. This allows distinguishing only carbides (white areas) and evaluating their morphology, amount, and distribution. Table 3 lists the results of carbide quantification in the as-cast condition, demonstrating the influence of the solidification rate imposed by the different Y-block thicknesses. As the Y-block thickness increased, carbides were enlarged and the content was reduced due to the decrease in the solidification rate.

Figure 4 shows the four matrix microstructures (optical microscopy) studied, in this case taken from the 25-mm Y-block. Figure 4a depicts a fully pearlitic matrix obtained in the as-cast condition (Pearlitic Ductile Iron (PDI) samples), Fig. 4b shows a martensitic matrix obtained by quenched and tempered (Q&T) (martensitic ductile iron (MDI) samples), and Figs. 4c and 4d show the two ausferritic matrices obtained by austempering at $T_a = 280$ and 360°C (CADI-280 and CADI-360), respectively.

Heat treatment not only promotes matrix microstructure modifications but changes the carbide content due to the partial dissolution taking place during the austenitizing stage of the Q&T and austempering heat treatment cycles. Table 3 lists the carbide content values after heat treatments, revealing the highest dissolution in the thin 12.5-mm Y-block and no dissolution in the 75-mm-thick Y-block.

When casting thickness increases and the solidification rate decreases, more time is allowed for diffusion of metallic atoms. Hence, microsegregation is more evident, promoting higher alloyed carbides with higher stability (Laino, et al. *(8)*; Caldera, et al. *(16)*). To verify this, semiquantitative chemical analyses of carbides were carried out by EDS, yielding the results provided in Table 4. As can be observed, as thickness increased, the quantity of the alloying elements in the carbides tended to increase as well, particularly Cr, given the higher microsegregation effect. Indeed, these results are in line with the lower carbide dissolution observed as the Y-block thickness increased, as presented in Table 3.

### Mechanical Properties

*Hardness and Impact Tests*

Figure 5 shows the results of the hardness tests undertaken for all the material combinations of Y-block thicknesses and matrix

TABLE 2—HEAT CHEMICAL COMPOSITION (WT%, FE BALANCE)

| C | Si | Mn | S | P | Mg | Cu | Cr | CE |
|---|---|---|---|---|---|---|---|---|
| 3.3 | 2.4 | 0.4 | 0.016 | 0.015 | 0.026 | 1.2 | 2.0 | 4.1 |

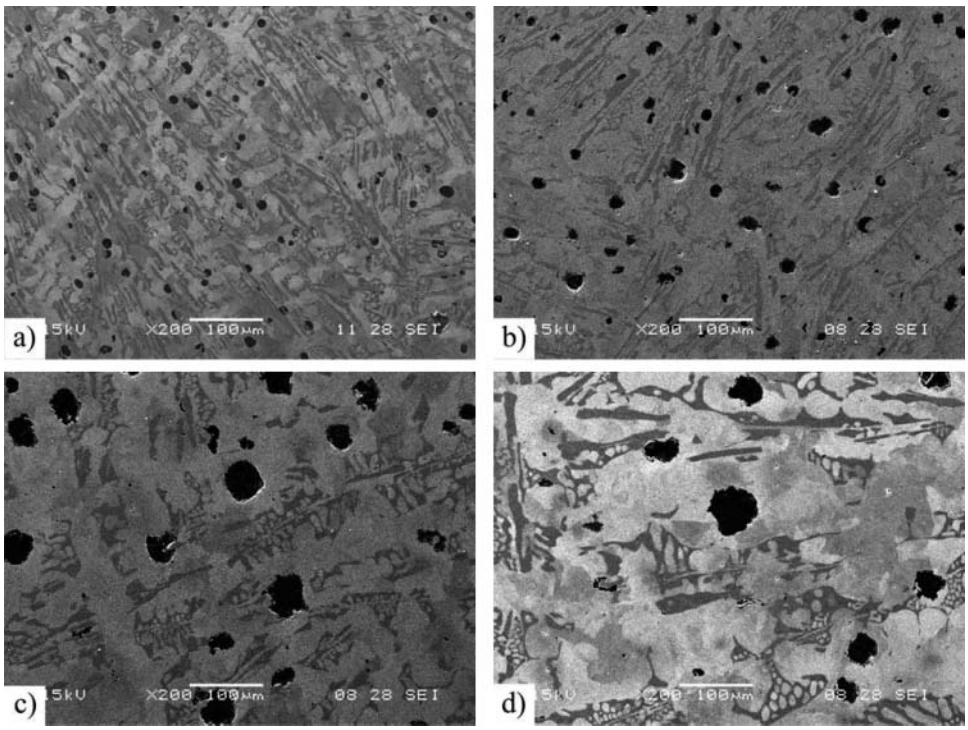


**Fig. 2—Scanning electron microscopy images of the microstructures for different Y-block thicknesses in the as-cast condition: (a) 12.5 mm, (b) 25 mm, (c) 50 mm, and (d) 75 mm. Etching was performed with 2% nital.**

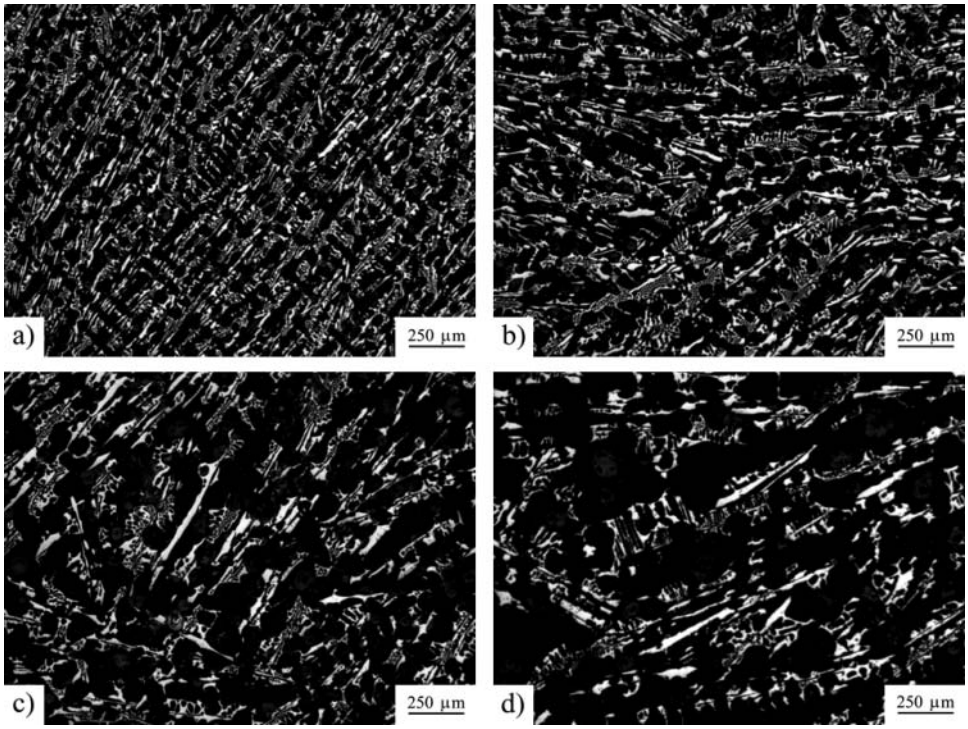


**Fig. 3—Carbides characteristics (white areas) for different Y-block thicknesses: (a) 12.5 mm, (b) 25 mm, (c) 50 mm, and (d) 75 mm. Etching was performed with 10% ammonium persulfate. After optical microscopy.**

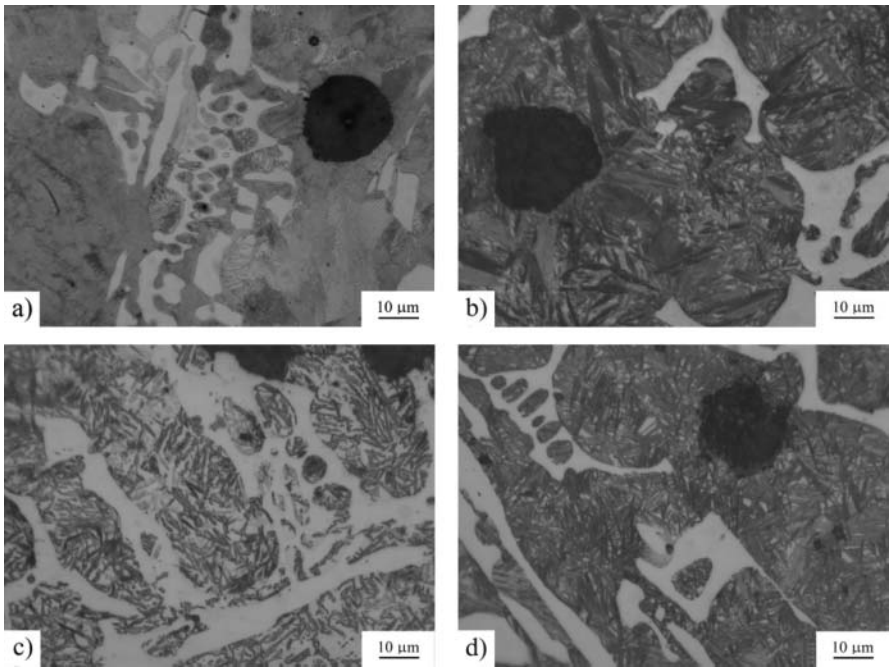


**Fig. 4—Optical matrix micrographs for 25-mm Y-block: (a) pearlitic, (b) martensitic, (c) ausferritic CADI-280, and (d) ausferritic CADI-360.**



microstructure variants evaluated, reflecting that hardness decreased as carbide content decreased. Figure 5 also illustrates the influence that the matrix type had on hardness. The hardest specimens were those with a martensitic matrix (MDI) followed by the ausferritic CADI-280, the ausferritic CADI-360, and, finally, the as-cast pearlitic matrix. The MDI variant with the smallest thickness (12.5 mm) had the highest hardness value, and the lowest hardness was obtained for the PDI variant with the greatest thickness (75 mm).

The microindentation tests demonstrated that the matrix hardness values were 675 HV for martensite, 500 HV for the ausferrite austempered at $T_a = 280°C$, 380 HV for the ausferrite austempered at $T_a = 360°C$, and 325 HV for the as-cast pearlite. The carbides' hardness was almost 1,100 HV for all material variants. This value was consistent with the expected type of carbide $M_3C$, which is basically $Fe_3C$ with Cr and Mn replacing Fe, as shown in Table 4.

The results for impact toughness measured with Charpy tests are shown in Fig. 6. First, it can be seen that the presence of carbide led to a large decrease in impact toughness (about 80–100 J), compared to the reference values of the different ADI grades,

TABLE 4—AMOUNT OF ALLOYING ELEMENTS, CR AND MN, IN THE CARBIDES FOR DIFFERENT Y-BLOCK THICKNESSES

| | Element (wt%) | |
|---|---|---|
| Y-Block Thickness (mm) | Cr | Mn |
| 12.5 | 2.2 | 0.86 |
| 25.0 | 3.6 | 0.95 |
| 50.0 | 4.3 | 0.97 |
| 75.0 | 4.4 | 1.1 |

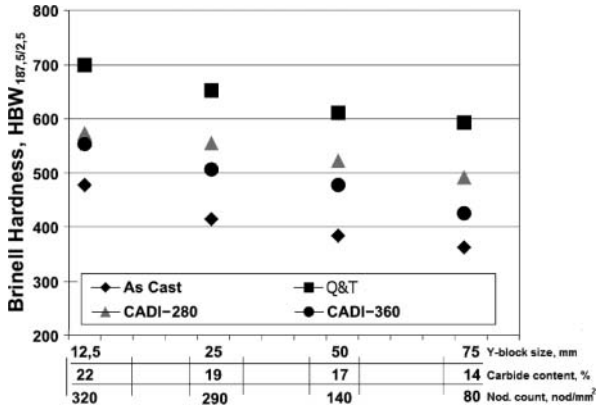


**Fig. 5—Hardness values ($HBW_{2.5/187.5}$) for all combinations of Y-block thicknesses and matrix microstructures.**

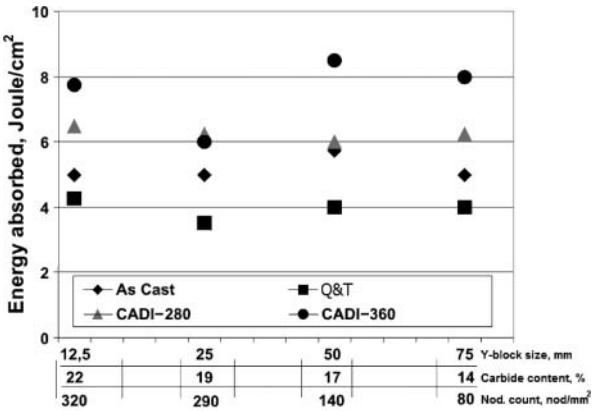


**Fig. 6—Impact toughness values for all combinations of Y-block thicknesses and matrix microstructures.**

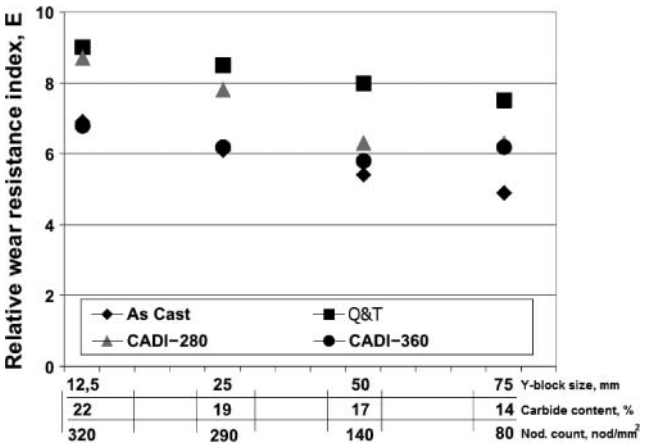


**Fig. 7—Relative wear resistance index (*E*) versus Y-block thickness for all matrix variants evaluated.**

according to ASTM A897M. It was be observed that as the Y-block thickness increased, the impact toughness remained mostly unchanged, proving that this property is not sensitive to the carbide content variations evaluated in this work. Nevertheless, the different matrices exerted their influence on this property, yielding the highest values for the CADI-360 samples, followed by CADI-280, PDI, and MDI variants.

The ausferrite obtained by austempering at $T_a = 360°C$ was the toughest phase of all of those studied in this work. However, previous works by the authors (Basso, et al. *(17)*) reported a detrimental effect on impact toughness when the section size was increased in carbide-free ADI. This difference was attributed to the presence of free carbides in the structure. Indeed, the presence of this hard and fragile phase significantly decreased the impact toughness, because it provided a preferential path for crack propagation during the fracture process, masking the potential effect of cast part size on these properties.

### *Abrasive Wear Resistance*

Figure 7 illustrates the relative wear resistance index value, $E$, as a function of Y-block thickness for all matrix microstructures. It can be seen that the highest relative wear resistance index, $E \sim 9.0$, was obtained for MDI samples taken from 12.5-mm Y-blocks and that the lowest value, $E \sim 4.9$, corresponded to the 75-mm as-cast PDI samples. The difference between the highest and lowest $E$ values for each different matrix was about $\Delta E \geq 1.5$, except for the CADI-360 variant (Fig. 7), thereby demonstrating the influence of carbide content and distribution on wear resistance.

Considering that the hardness of a material is defined as its resistance to penetration, this property can be considered to affect abrasive particles penetration and hence the volume removed by an abrasive particle when sliding to create a scratch (Khrushchov and Babiechev *(18)*); that is, higher hardness results in higher abrasion resistance. In this case, the influence of the matrix microstructure and its corresponding hardness can also be observed in Fig. 7, where the highest wear resistance (under the present experimental conditions) corresponds to the matrix with the highest hardness and the lowest wear resistance corresponds to that of the matrix with the lowest hardness. This type of relation between hardness and abrasive wear resistance is not always applicable, but it has been previously reported for the tribosystem used in

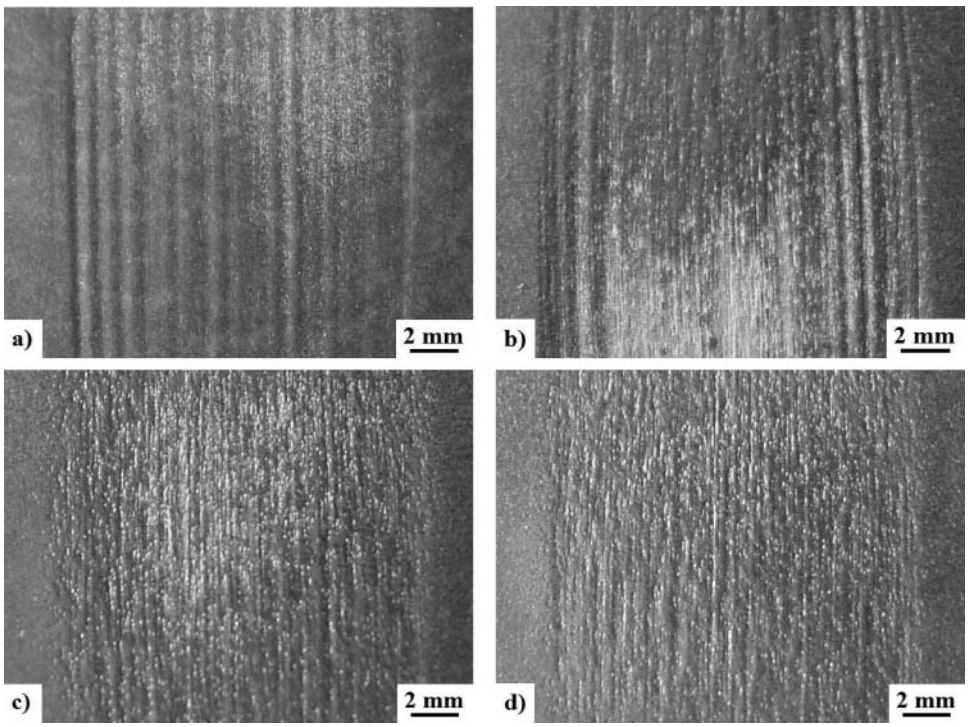


**Fig. 8—Wear scars obtained from the abrasion tests for different Y-block thicknesses: (a) 12.5 mm, (b) 25 mm, (c) 50 mm, and (d) 75 mm.**

this study (Laino, et al. *(8)*, *(11)*; Ceccarelli, et al. *(12)*; Giacchi, et al. *(13)*).

These results show that the abrasive wear resistance can be improved by the addition of reinforcing particles, in this case, iron carbides with a typical hardness of about 1,100 HV. Previous works comparing the wear resistance of ductile iron without carbides (used as the reference material) and with carbides in similar amounts to those used herein showed an increase in the wear resistance from $E \sim 1.0$ up to $E \sim 2.5$, respectively (Laino, et al. *(7)*, *(8)*, *(11)*; Ceccarelli, et al. *(12)*).

Figures 8a–8d illustrate the wear scars obtained from the abrasion tests performed and show the influence of microstructure on topography. The higher carbide content and shorter distance between carbides of the 12.5-mm-thick Y-block promoted a smoother wear scar compared to that of the 75-mm Y-block, where the size and distance between carbides allowed the abrasive particles to preferentially penetrate and abrade the matrix.

From Fig. 7 it is also possible to note a typical trend toward a decrease in $E$ as thickness increased. Nevertheless, when comparing the response of both CADI variants, the values of the 75-mm Y-block were very similar or even slightly higher than those of the 50-mm Y-block. This response was ascribed to the increasing retained austenite contents ($\gamma_{ret}$) with thickness, from $\gamma_{ret} \sim 26\%$ for 12.5 mm in CADI-280 up to $\gamma_{ret} \sim 46\%$ for 75 mm in CADI-360, as presented in Figs. 9 and 10. The $\gamma_{ret}$ arises from the contribution of the so-called reacted austenite (present in the ausferrite) and the so-called nonreacted austenite (present at the LTF zones, stabilized by the higher contents of Cr and Mn, not transforming on cooling; Laino, et al. *(8)*; Rivera, et al. *(19)*, *(20)*).

Austenite is a metastable phase and, as such, may transform into martensite ($\gamma \rightarrow$ M) under abrasive wear conditions, due to the strain imposed by the abrasive particles on the matrix and thus promoting a stress-assisted or strain-induced transformation, already demonstrated in wear and fracto-mechanical tests in steels (Vourinen, et al. *(21)*; Putatunda *(22)*) and ADI

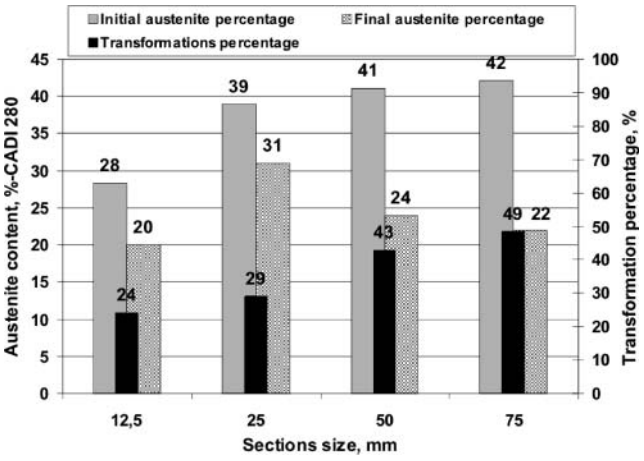


**Fig. 9—Retained austenite under unworn and worn conditions and austenite-to-martensite transformation percentage for CADI-280 depending on Y-block thickness.**

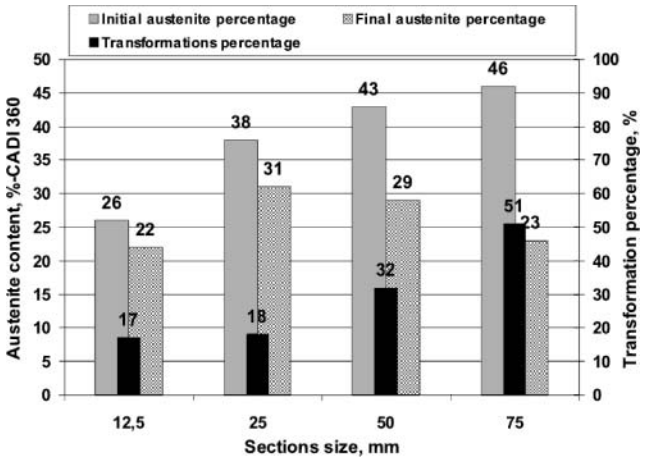


**Fig. 10—Retained austenite under unworn and worn conditions and austenite-to-martensite transformation percentage for CADI-360 depending on Y-block thickness.**

(Dommarco, et al. *(5)*; Shepperson and Allen *(6)*; Francucci, et al. *(15)*).

To evaluate and quantify the $\gamma \rightarrow$ M transformation as a consequence of abrasion, XRD tests were also performed after the wear tests on CADI-280 and CADI-360 samples, as shown in Figs. 9 and 10, respectively. $\gamma \rightarrow$ M transformation was present in both CADI variants, and the austenite transformation percentage, $\Delta\gamma$, increased as the wall thickness increased, with maximum values around $\Delta\gamma \sim 50\%$ for both austempering temperatures.

Therefore, the highest $\Delta\gamma$ values coincided with the highest $E$ values for the CADI samples from the 75-mm Y-blocks with respect to those from the 50-mm Y-blocks.

Therefore, different factors affect $E$, which are dependent on the Y-block thickness as well as on the matrix obtained after heat treatment, such as carbide content, austenite content, nodule count, and matrix hardness.

## CONCLUSIONS

The addition of Cr to the melt allowed the formation of free carbides during solidification, but their size, distribution, and chemical composition were affected by the solidification rate. It was observed that as the section size increased—that is, the solidification rate decreased—the amount of carbides decreased as well but the percentage of both Cr and Mn in carbides increased. Nodule count also decreased as the section size increased.

It was also noticed that during the austenizing step of heat treatments, carbides partially dissolved depending on their degree of alloying, ranging from 4% for the 12.5-mm Y-block to 0% for the 75-mm Y-block.

As a general rule, when the section size increased, the impact toughness remained unchanged. Fully ausferritic matrices austempered at 360°C (CADI-360) yielded the highest impact toughness values. The ausferrite obtained by austempering at this temperature was the toughest phase of all those analyzed in this work.

It was shown that the abrasive wear resistance was improved by the presence of carbides, whose main effect was to increase

the material hardness and hence to reduce the abrasive particle penetration depth. For a given amount, size, and distribution of carbides, the matrix microstructure also plays an important role. In fact, under the current experimental conditions the highest $E$ value was obtained for the 12.5-mm Y-block with a martensitic matrix, in coincidence with the highest hardness value.

$E$ values for the highest Y-block thicknesses (50 and 75 mm) tended to stabilize for CADI-280 and CADI-360 variants. This was explained by the increasingly higher austenite content of these variants, which transformed into martensite due to their plasticity associated with abrasion.

## REFERENCES


(1) Magalhaes, L. and Seabra, J. (1998), "Wear and Scuffing of Austempered Ductile Iron Gears," *Wear*, **215**, pp 237–246.

(2) Straffelini, G., Giuliari, C., Pellizzari, M., Venerib, E., and Bronzato, M. (2011), "Dry Rolling–Sliding Wear of Austempered Cast Iron," *Wear*, **271**, pp 1602–1608.

(3) Dommarco, R. C., Bastias, P. C., Dall'O, H. A., Hahn, G. T., and Rubin, C. (1998), "Rolling Contact Fatigue (RCF) Resistance of Austempered Ductile Iron (ADI)," *Wear*, **221**, pp 69–74.

(4) Yang, J. and Putatunda, S. (2005), "Effect of Microstructure on Abrasion Wear Behavior of Austempered Ductile Cast Iron (ADI) Processed by a Novel Two-Step Austempering Process," *Materials Science and Engineering A*, **406**, pp 217–228.

(5) Dommarco, R., Galarreta, I., Ortíz, H., David, P., and Maglieri, G. (2001), "The Use of Ductile Iron for Wheel Loader Bucket Tips," *Wear*, **249**, pp 100–107.

(6) Shepperson, S. and Allen, C. (1998), "The Abrasive Wear Behaviour of Austempered Spheroidal Cast Irons," *Wear*, **121**, pp 271–287.

(7) Laino, S., Sikora, J. A., and Dommarco, R. C. (2008), "Development of Wear Resistant Carbidic Austempered Ductile Iron (CADI)," *Wear*, **265**, pp 1–7.

(8) Laino, S., Sikora, J. A., and Dommarco, R. C. (2009), "Influence of Chemical Composition and Solidification Rate on the Abrasion and Impact Properties of CADI," *ISIJ International*, **49**, pp 1239–1245.

(9) Rebasa, N., Dommarco, R., and Sikora, J. (2002), "Wear Resistance of High Nodule Count Ductile Iron," *Wear*, **253**, pp 855–863.

(10) Dommarco, R. C., Sousa, M. E., and Sikora, J. A. (2004), "Abrasion Resistance of High Nodule Count Ductile Iron with Different Matrix Microstructures," *Wear*, **257**, pp 1185–1192.

(11) Laino, S., Sikora, J. A., Dommarco, R. C. (2010), "Wear Behavior of CADI Operating under Different Tribosystems," *ISIJ International*, **50**, pp 418–424.

(12) Ceccarelli, B., Dommarco, R., Martinez, R., and Martinez Gamba, M. (2004), "Abrasion and Impact Properties of Partially Chilled Ductile Iron," *Wear*, **256**, pp 49–55.

(13) Giacchi, J. V., Martínez, R. A., Martínez Gamba, M. R., and Dommarco, R. C. (2007), "Abrasion and Impact Properties of Partially Chilled Gray Iron," *Wear*, **262**, pp 282–291.

(14) Laino, S., Ortíz, H. R., and Dommarco, R. C. (2009), "The Influence of Austempering Temperature on the Wear Resistance of Ductile Iron under Two Different Tribosystems," *ISIJ International*, **49**, pp 132–138.

(15) Francucci, G., Sikora, J. A., and Dommarco, R. C. (2008), "Abrasion Resistance of Two Step Austempered Ductile Iron," *Materials Science and Engineering A*, **485**, pp 46–54.

(16) Caldera, M., Rivera, G., Boeri, R., and Sikora, J. (2005), "Precipitation and Dissolution of Carbides in Low Alloy Ductile Iron Plates of Varied Thickness," *Materials Science and Technology*, **21**, pp 1187–1191.

(17) Basso, A., Martinez, R., and Sikora, J. (2009), "Influence of Section Size on Dual-Phase ADI Microstructure and Properties: Comparison with Fully Ferritic and Fully Ausferritic Matrices," *Materials Science and Technology*, **25**, pp 1271–1278.

(18) Khrushchov, M. and Babiechev, M. (1958), "An Investigation of the Wear of Metals and Alloys by Rubbing on an Adhesive Surface," *Friction and Wear in Machinery*, **12**, pp 1–13.

(19) Rivera, G., Boeri, R., and Sikora, J. (2002), "Revealing and Characterizing Solidification Structure of Ductile Cast Iron," *Materials Science and Technology*, **18**, pp 691–697.

(20) Rivera, G., Boeri, R., and Sikora, J. (1999), "Influence of the Solidification Microstructure on the Mechanical Properties of Ductile Iron," *International Journal of Cast Metals Research*, **11**, pp 533–538.

(21) Vourinen, E., Pino, D., Lundmark, J., and Prakash, B. (2007), "Wear Characteristic of Surface Hardened Ausferritic Si-Steel," *Proceedings of the Sino-Swedish Structural Materials Symposium*. Beijing, China, 18–19 September, 2007.

(22) Putatunda, S. (2003), "Influence of Austempering Temperature on Microstructure and Fracture Toughness of a High-Carbon, High-Silicon and High-Manganese Cast Steel," *Materials & Design*, **24**, pp 435–443.